Images of interlayer vortices and *c*-axis penetration depth of high-T_c YBa$_2$Cu$_3$O$_{7-y}$ superconductor

Ienari Iguchi,[1,2] Tomohiro Takeda,[2] Tetsuji Uchiyama,[2] Akira Sugimoto,[3] and Takeshi Hatano[1]

[1]*Nanomaterials Laboratory, National Institute for Materials Science, Sengen 1-2-1, Tsukuba 305-0047, Japan*
[2]*Department of Physics, Tokyo Institute of Technology, 2-12-1 O-okayama, Meguro-ku, Tokyo 152-8551, Japan*
[3]*Faculty of Integrated Arts and Sciences, Hiroshima University, 1-7-1Kagamiyama, Higashi-Hiroshima 739-8521, Japan*

The measurements on the magnetic image of interlayer vortices are performed for the high-T_c YBa$_2$Cu$_3$O$_{7-y}$(110) thin film using a high sensitive scanning SQUID microscopy. Clear images of aligned giant interlayer vortices are observable. For the majority of vortices, using the London model, the *c*-axis penetration depth is estimated to be about 20 μm at 3 K. The temperature dependence of λ_c is obtained from the observed vortex images at different temperatures, whose behavior is in good agreement with those of the microwave cavity measurement.

It is well known that high-T_c superconductors has a structure with the stacked two-dimensional superconducting planes and behave like two dimensional superconductors because of their large anisotropy. The large anisotropy yields the large difference between the London magnetic penetration depth in the *ab*-plane (λ_{ab}) and along the *c* axis (λ_c). The magnitude of λ_{ab} generally ranges from 0.1 μm to 0.5 μm, whereas the λ_c value for the interlayer vortices is very large for highly anisotropic superconductors. The latter is particularly important since it is directly related to the size of interlayer vortices in the *ab*-plane which attracted considerable attention for the basic study of vortex flow,[1–6] the superconductivity mechanism by the Anderson's interlayer tunneling model,[7,8] and the possible THz application of Josephson plasma phenomena[9–13] recently.

The λ_c value is indirectly determined from the measured Josephson plasma frequency ω_p by the relation $\omega_p = c/\sqrt{\varepsilon}\lambda_c$ where c is the speed of light and ε is the dielectric constant of the interlayer medium. ω_p is determined by microwave cavity measurements or infrared spectroscopy.[14–20] The dielectric constant ε has, however, some ambiguity. Besides, the measurements provide only the value of λ_c and does not provide any information on the structure of an interface vortex. λ_c largely depends on individual materials and the doping levels. Hence the direct measurement of λ_c is necessary.

Recent scanning SQUID spectroscopy (SSM) technique provides the direct measurement of the interlayer quantized vortices which allows the direct estimation of λ_c. Although the measurements on the pancake vortices, the Josephson vortices at the grain boundaries and the half integer vortex at the tricrystal boundary in the *c*-axis oriented films or crystals are abundant,[21–27] there exist only a few reports on the measurement of λ_c which is also limited to specific thallium and mercury cuprates [$\lambda_c = 8$ μm for Hg-1201 (Ref. 28) and $\lambda_c = 17 – 19$ μm for Tl-2201 (Ref. 29)]. Besides, the measurements were performed only at 4.2 K. There is no report on the commonly used yttrium and bismuth cuprates, probably due to the fact that the preparation of a smooth *a-b* or *a-c* plane surface for single crystal samples and, also the growth of high quality non-*c*-axis oriented films are not easy. Note that the preparation of the *c*-plane oriented smooth surface for single crystals or the growth of the *c*-axis oriented films

is much easier. From the viewpoint of basic study of vortices in anisotropic cuprates and device application, it is also very important to investigate the structure of interlayer vortices directly at higher temperature.

Here we demonstrate the first measurement on the magnetic images of interlayer vortices in the YBa$_2$Cu$_3$O$_{7-y}$(YBCO)(110) thin film using the SSM. By this measurement, we determined the *c*-axis penetration depth for the YBCO material. The clear image of interlayer vortices was observable without significant broadening of the vortex shape up to about 50 K. The temperature dependence of λ_c appeared not to be linear as expected for a *d*-wave pairing state, suggesting the involvement of incoherent process as suggested by Hosseini *et al.*[17,18]

The SSM made use of Nb SQUID and had a spatial resolution limited by the input coil diameter of 10 μmϕ. Both the SQUID and the pick-up coil were mounted on a Si chip set on a cantilever which was oriented an angle $\theta \sim 5°$ from parallel to the sample; and scanned with the tip not touching the sample. The SQUID resolution was 5×10^{-6} Φ_0 Hz$^{-1/2}$, and the scanning of sample stage was done by three stepping motors along the *x*, *y*, and *z* axes. The detector picked up the magnetic flux through the pickup coil normal to the sample surface, i.e., the *z* direction. The sample-pickup coil distance was about 3 μm as calculated from fits to data on Abrikosov vortices. The magnetic image of pancake vortices along the *c* axis is limited by the size of the pickup coil which is much greater than λ_{ab}. On the other hand, the spreading of interlayer vortices in the *ab*-plane gives the estimate for λ_c. The sample temperature was variable between 3 K and 90 K. The use of a permalloy magnetic shield reduced the background magnetic field to be about 0.2 μT. A small magnetic field could be generated by the coil wound around the sample, if necessary.

The sample was fabricated by depositing YBa$_2$Cu$_3$O$_{7-x}$(110) thin films on the SrTiO$_3$(STO)(110) single crystal substrates using a pulsed laser deposition technique. The lattice constant of STO is 0.391 nm. The *c*-axis length of YBCO is 1.17 nm, which corresponds to just three times of STO(110) lattice constant. The growth of YBCO(110) thin films was done in the following way. Using a KrF excimer laser with wavelength of 248 nm, energy of
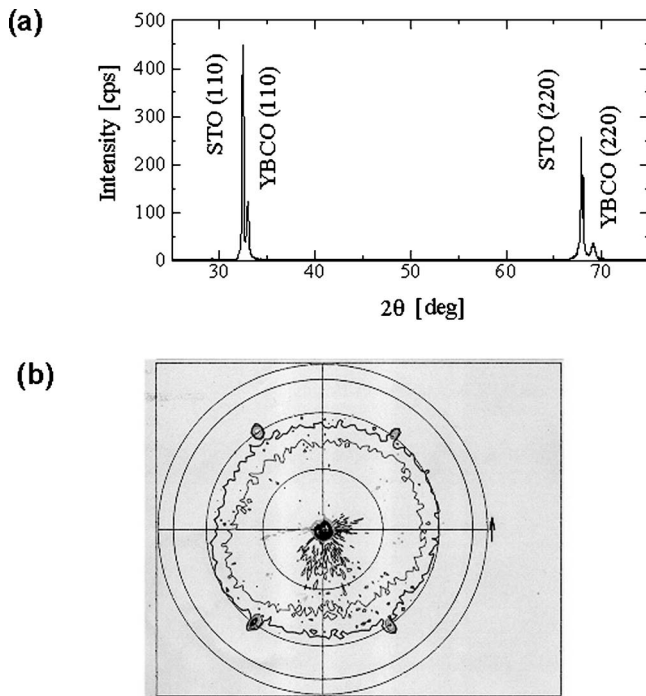
(a)

(b)

FIG. 1. (a) X-ray diffraction pattern for the (110) YBCO film, (b) x-ray pole figure of the (110) YBCO film.

250–300 mJ and the repetition rate of 2 Hz, a YBCO film was deposited at 690 °C for 10 min under 0.4 Torr oxygen pressure. Subsequently the substrate temperature was increased up to 800 °C and an additional YBCO film was deposited again for 30 min. In this process, first an *ab*-plane

oriented YBCO film was grown at lower deposition temperature, thereafter the transition temperature T_c of the film was improved by increasing the deposition temperature higher. This method is the so-called "template method." The thin-film sample thus fabricated was mounted on the sample holder using epoxy. The *c* axis lies in the film and the (110) face was aligned vertically. T_c of the film was 83 K.

Figure 1(a) shows the x-ray diffraction pattern of the YBCO film. The YBCO(110) and (220) peaks are markedly pronounced, indicating the strong orientation along the (110) direction. To exclude the possibility of (103) peaks, the polar x-ray figure [Fig. 1(b)] was also recorded, which yielded four peaks confirming the (110) orientation.

Figures 2(a) and 2(b) show two examples of the observed three dimensional SSM magnetic images of interlayer vortices in the YBCO(110) film at 3 K in the scanning area of $300 \times 300~\mu m^2$ and $250 \times 250~\mu m^2$, respectively. Figure 2(a) corresponds to the data under the least background magnetic field, whereas Fig. 2(b) corresponds to those under a slightly higher magnetic field for which the flux distribution is denser. The presence of the aligned long vortices along the *y*-axis direction is evident. The *x* axis corresponds to the *c*-axis direction of the YBCO(110) film. Some of the observed vortices are clearly overlapped with each other, particularly for Fig. 2(b), due to the close presence in space. The nearly uniform appearance of interlayer vortices in the large area indicates that the fabricated YBCO(110) film was of high quality, although some locally disordered vortices are seen probably due to the stacking faults in the scale of several tens of microns. For comparison, the magnetic image of the pinned pancake vortices observed in the *c*-axis oriented YBCO(001) film in the scanning area of $320 \times 200~\mu m^2$ is
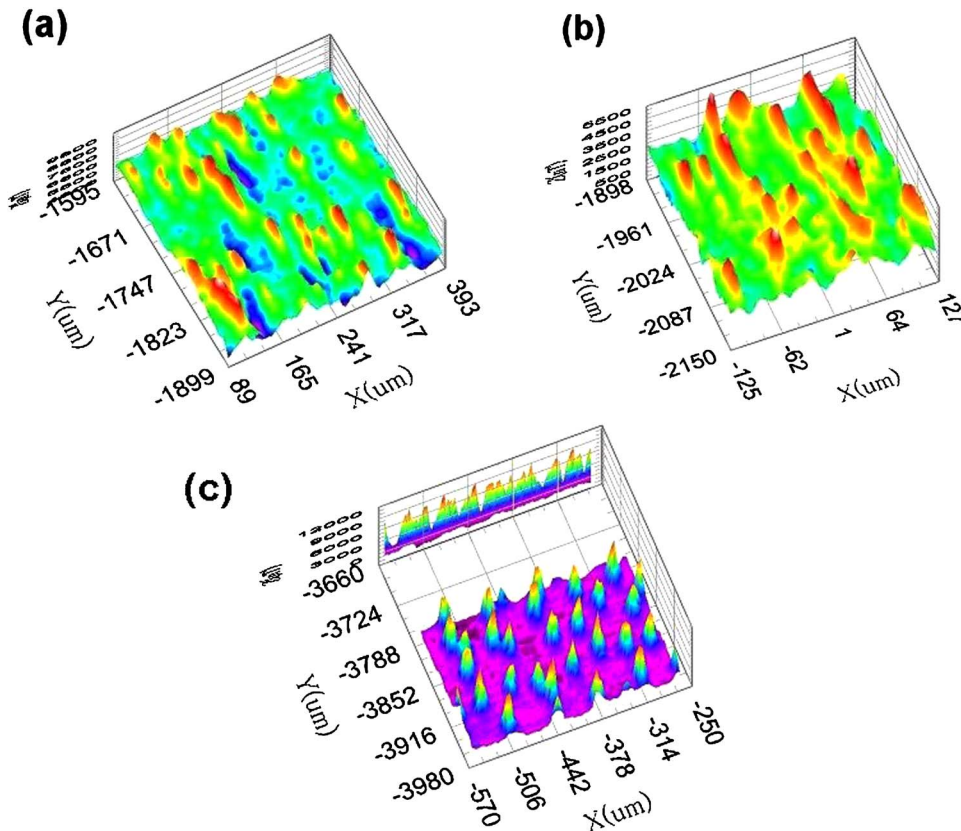
(a)

(b)

(c)

FIG. 2. (Color online) (a), (b) Examples of three-dimensional SSM magnetic image of the YBCO(110) film at 3 K, (c) example of SSM magnetic image of the *c*-axis oriented YBCO(001) film at 3 K. While long aligned interlayer vortices are observable in (a) and (b), only round pancake vortices are visible in (c).

3.0K   **20.5K**
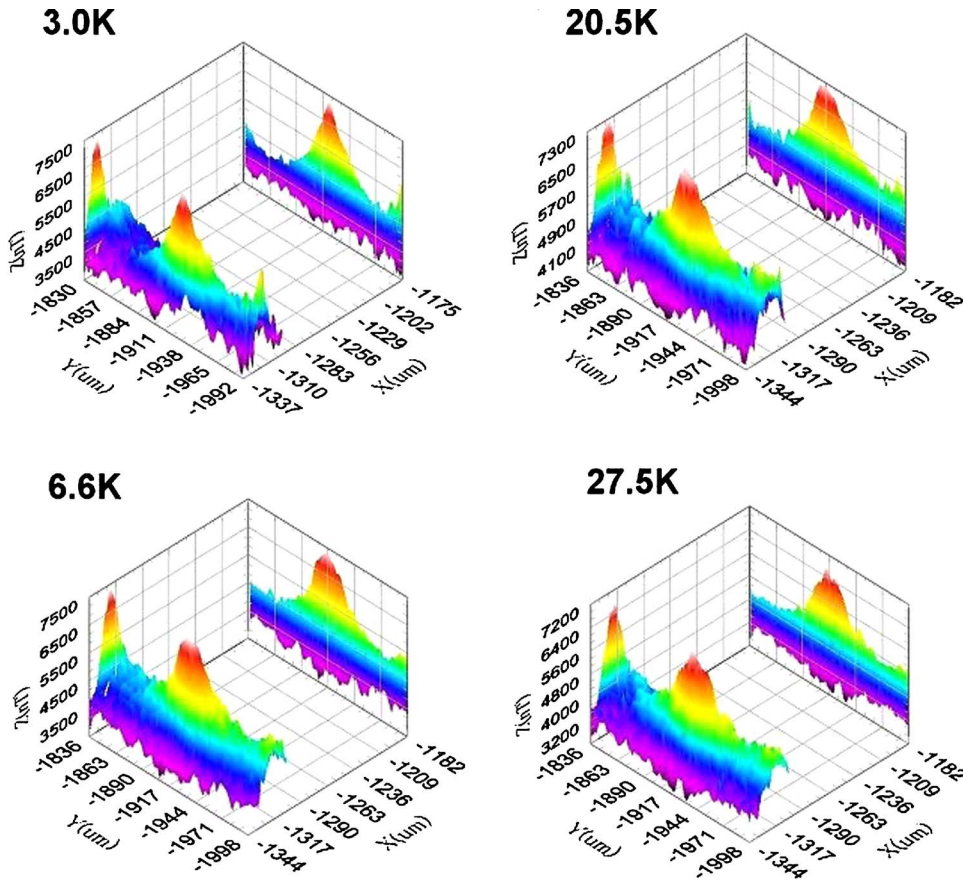
6.6K   **27.5K**

FIG. 3. (Color online) Three-dimensional SSM magnetic image of an isolated interlayer vortex at different temperatures.

shown in Fig. 2(c). In contrast to the round vortices in the *c*-axis oriented film, the aligned interlayer vortices are quite long. It is found by integrating the observed individual flux signal that one interlayer vortex approximately carries one quantum flux unit $\Phi_0 = h/2e$.

Figure 3 shows a representative single interlayer vortex at different temperatures. They appeared to be slightly asymmetric in space due to the overlapping effect of background magnetic field from the neighboring vortices. The single vortex image was clearly visible up to about 50 K, showing that the isolated interlayer long vortices are stably present. Above 50 K, the vortex structure was much more smeared and almost disappeared probably due to the fact that the vortex is more weakly pinned as the temperature is increased.

The magnetic-field penetration depth λ_c was estimated by using the following London model for the anisotropic superconductor[30,31]

$$B_z(x, y, z = 0, \lambda_c, \lambda_{ab}) = \frac{\Phi_0}{2\pi\lambda_{ab}\lambda_c} K_0(R),$$

$$R = \left(\frac{x}{\lambda_c}\right)^2 + \left(\frac{y}{\lambda_{ab}}\right)^2, \qquad (1)$$

where $K_0(x)$ is the modified Bessel function of the zeroth order. The field is summed over the area of the pickup coil. In the data fitting process, two parameters were assumed. One is the sample-pickup coil distance z which determines the magnitude of magnetic field of the vortex image. From

the data of the independent measurement on the isolated pancake vortex, we assumed $z = 3$ μm and $\lambda_{ab} \approx 0.1$ μm. Note that the value of λ_{ab} does not affect λ_c seriously since $\lambda_c \gg \lambda_{ab}$.

To estimate λ_c, the data fitting process was done using Eq. (1) and the peak data nearly free from the background magnetic field. For the majority of vortices, the result yielded $\lambda_c = 19.5 \pm 1.5$ μm at 3 K. For a few vortices inside the scanning area, however, a smaller penetration depth of $\lambda_c = 11 \pm 1$ μm was also observable. The observed values are much greater than that of Hg-1201,[28] much smaller than the expected ones of Bi2212 or Bi2223, but comparable to that of Tl-2201 (Ref. 29) by the scanning SQUID microscopy. They are a factor of 5 or about one order of magnitude greater than those reported for near optimally-doped YBCO superconductors with T_c of about 80 K ($\lambda_c \sim 1.5$ μm) obtained by far-infrared measurements or microwave cavity measurements,[14,17] although a large value of 29 μm is reported for an underdoped YBCO with $T_c = 20$ K.[18] As for the origin of large discrepancy, we checked the data analysis very carefully, but no error was found, precluding such possibility. Because of the large λ_c value much greater than the diameter of SQUID input coil, the observed value is quite reliable, in contrast to those of λ_c or λ_{ab} values much smaller than the SQUID spatial resolution. Kirtley *et al.*[31] calculated the spreading effect of vortices at the superconducting surface, but this effect did not give a large change corresponding to the observed penetration depth. We point out that, although the previous electromagnetic measurements apparently provide a common value for λ_c, we still cannot pre-
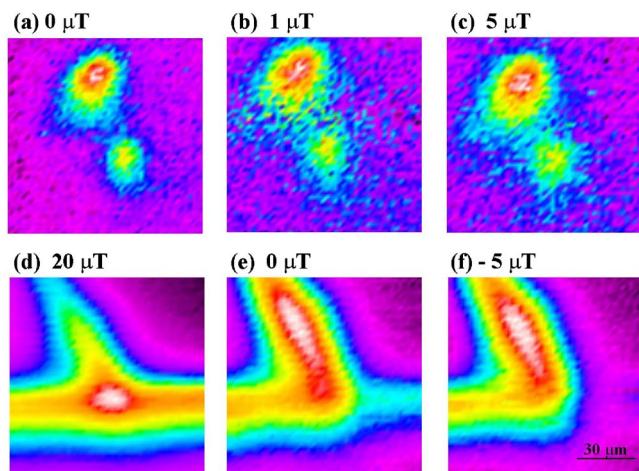
FIG. 4. (Color online) Magnetic images (top view) for a *c*-axis oriented YBCO thin film deposited on a tricrystal substrate under different external magnetic field. Note that large and small vortices seen in (a)–(c) are a Josephson quantum vortex and a half flux quantum vortex at the tricrystal point typical for a *d*-wave superconductor, respectively. The intrusion of external magnetic field along the grain boundaries (d)–(f) produced long strip images different from a single vortex.

clude the possibility that the measured λ_c did not reflect the correct value since they only give some spatially averaged value of λ_c on the surface of a YBCO single crystal which is definitely affected by the oxygen deficiency effect, crystal defects [stacking faults, i.e., possible contributions from λ_{ab} ($\approx 0.15~\mu$m)] or impurities.

To demonstrate the validity of our measurement technique further, we have performed an additional measurement on a *c*-axis oriented YBCO thin film deposited on a tricrystal crystal substrate. This tricrystal geometry was the same as that of previous measurements used for the proof of *d*-wave superconductivity for oxide cuprates.[21,23,26] Figure 4 shows an example of the observed magnetic images (top view) under different external magnetic fields at 3 K. When the field is small, a clear half flux quantum vortex typical of a *d*-wave superconductor at the tricrystal point and a Josephson vortex are recognizable in Figs. 4(a)–4(c). The observed half flux quantum appeared as a smaller magnetic image. The size of the observed magnetic images nearly agrees with that calculated from simulation obtained by assuming the input-coil diameter of 10 μmϕ. Under the field of 20 μT [Fig. 4(d)],

the external field penetrated into the grain boundaries, which produced long magnetic images corresponding to the same scale length of the interlayer vortices. Figure 4(e) shows the magnetic image when the external field was turned off, for which the trapped vortices (overlapped) in the grain boundaries are evident. Figure 4(f) shows a magnetic image when the field was applied to opposite direction. The above result justifies our measurement technique for observation of large interlayer vortices. The similar magnetic images have been also obtained in the bicrystal grain boundaries in the *d*-wave YBCO superconductors.[27]

Based on the above discussions and the result of Fig. 4, apart from the validity of the previously obtained data,[14,17] we conjecture that the discrepancy may arise from the samples used. In contrast to single-crystal samples used for all the other λ_c measurements, our measurement used epitaxially grown YBCO(110) thin films. Thin films generally have the grain structure. In fact, the observed supercurrent density in the *ab*-plane ($\sim 10^4$ A/cm^2) was about two orders of magnitude smaller than that of optimally-doped single crystals, although the T_c was 83 K. The observed broad superconducting transition ($\Delta T_c = 10$ K) reflects such situation. The interlayer vortices are penetrated into weak superconducting regions selectively in order to minimize the energy loss by flux penetration, hence more easily pinned at the grain boundaries or, crystal defects, or twin boundaries, or impurities within the grain. In the weak superconducting region, the order parameter is significantly reduced, which works as a Josephson junction or a weak junction. This also yields a longer penetration depth for λ_c. The two orders of magnitude different in the critical current density gives the right order of magnitude for the observed λ_c since λ_c becomes inversely proportional to the square root of the current density. By assuming that the λ_c values obtained in the previous measurements are correct, we come to a conclusion that the vortices with $\lambda_c \sim 20~\mu$m possibly corresponds to those pinned at grain boundaries, while those with $\lambda_c \sim 11~\mu$m may be the interlayer vortices pinned at crystal defects, twin boundaries, or impurities within the grain. We consider that the qualitative feature of these vortices is similar to those unpinned as far as the interlayer vortices are concerned. The λ_c in the weak coupling region is a very important physical property since it is closely related to the Josephson penetration depth, hence is considered to be a fundamental property of a high-T_c oxide superconductor which may be comparable to bulk λ_c under various doping levels.
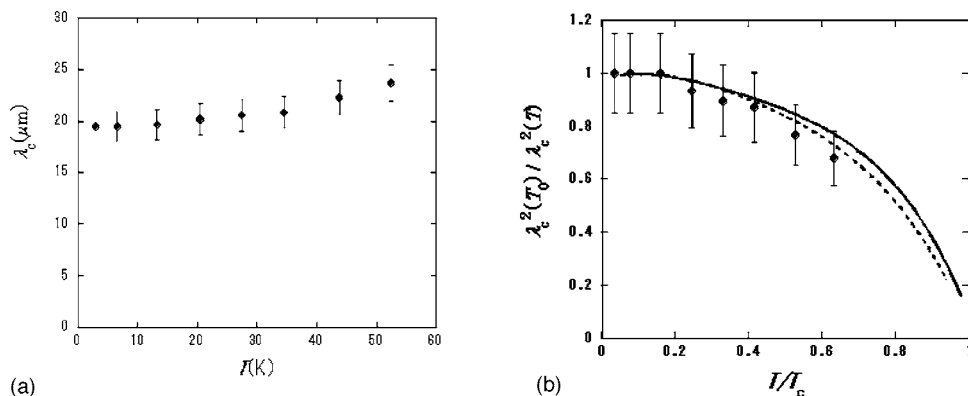

FIG. 5. (a) Temperature dependence of the *c*-axis penetration depth. (b) $1/\lambda_c^2(T)$ value normalized by the value $\lambda_c^2(T_0)$ at the lowest measured temperature T_0 as a function of temperature. Note that the quantity $\lambda_c^2(0)/\lambda_c^2(T)$ is directly proportional to the superfluid density.

(a)

(b)

Figure 5(a) shows the temperature dependence of the c-axis penetration depth λ_c of about 20 μm calculated from the observed magnetic images at different temperatures by a data fitting process using Eq. (1). The result shows that λ_c increased by an amount of 20% at 52 K corresponding to the reduced temperature $T/T_c = 0.6$ and has no linear dependence on temperature seen in the ab plane whose behavior is expected for a d-wave pairing state. Figure 5(b) shows the temperature dependence of the quantity $\lambda_c^2(T_0)/\lambda_c^2(T)$ where $\lambda_c(T_0)$ is the measured value at the lowest measured temperature, together with those reported by the microwave cavity measurements. Note that the quantity $\lambda_c^2(T_0)/\lambda_c^2(T)$ is directly proportional to the superfluid density. The solid and dotted curves correspond to those of optimally-doped ($T_c \approx 92$ K) and undoped YBCO ($T_c \approx 20$ K) samples by Hosseini *et al.*,[17,18] respectively. Their results show that the qualitative feature of $1/\lambda_c^2$ curve has very little doping dependence. Although the error bar of the observed data were significantly large due to original scattered data in the SSM measurements, the qualitative feature agrees well with the previously reported data as expected. The $\lambda_c^2(T_0)/\lambda_c^2(T)$ curve has roughly T^2 behavior which is not related to the conventional Josephson behavior. This suggests that the c-axis transport is dominated by the incoherent processes as suggested by Ref. 17.

Since the anisotropy of YBCO material is smaller than that of Bi2212 and is closer to three dimensional structure, the Josephson plasma frequency f_p is expected to be much higher than that of Bi2212 (about 100 GHz). From the observed c-axis penetration depth, the Josephson plasma frequency $f_p = c/2\pi\sqrt{\varepsilon}\,\lambda_c$ is estimated to be about 0.8 THz by assuming $\varepsilon = 10$, which is promising to Terahertz frequency application.

In summary, we have shown the direct observation of interlayer vortices in YBCO material by a scanning SQUID microscope technique. The observed c-axis penetration depth appeared as about one order of magnitude longer than those of the other measurements, although the temperature dependent behavior was qualitatively similar. This discrepancy is reconciled by considering the pinning of interlayer vortices at the grain boundaries or crystal defects or impurities preferably.

[1] T. Koyama and M. Tachiki, Solid State Commun. **96**, 367 (1995).

[2] B. I. Ivlev, N. B. Kopnin, and V. L. Pokrovsky, J. Low Temp. Phys. **80**, 187 (1990).

[3] J. U. Lee, J. E. Nordman, and G. Hohenwarter, Appl. Phys. Lett. **67**, 1471 (1995).

[4] S. Ooi, T. Mochiku, and K. Hirata, Phys. Rev. Lett. **89**, 247002 (2002).

[5] A. E. Koshelev, Phys. Rev. B **66**, 224514 (2002).

[6] M. Ichioka, Phys. Rev. B **51**, 9423 (1995).

[7] P. W. Anderson, Science **268**, 1154 (1995).

[8] P. W. Anderson, Science **279**, 1196 (1998).

[9] M. Tachiki, T. Koyama, and S. Takahashi, Phys. Rev. B **50**, 7065 (1994).

[10] S. E. Shafranjuk and M. Tachiki, Phys. Rev. B **59**, 14087 (1999).

[11] K. Lee, W. Wang, I. Iguchi, M. Tachiki, K. Hirata, and T. Mochiku, Phys. Rev. B **61**, 3616 (2000).

[12] E. Kume, I. Iguchi, and H. Takahashi, Appl. Phys. Lett. **75**, 2809 (1999).

[13] M. Tachiki, M. Iizuka, K. Minami, S. Tejima, and H. Nakamura, Phys. Rev. B **71**, 134515 (2005).

[14] C. C. Homes, T. Timusk, D. A. Bonn, R. Liang, and W. N. Hardy, Physica C **254**, 265 (1995).

[15] H. Shibata and T. Yamada, Phys. Rev. B **54**, 7500 (1996).

[16] S. Tajima, J. Schutzmann, S. Miyamoto, I. Terasaki, Y. Sato, and R. Hauff, Phys. Rev. B **55**, 6051 (1997).

[17] A. Hosseini, S. Kamal, D. A. Bonn, Ruixing Liang, and W. N. Hardy, Phys. Rev. Lett. **81**, 1298 (1998).

[18] A. Hosseini, D. M. Broun, D. E. Sheehy, T. P. Davis, M. Franz, W. N. Hardy, Ruixing Liang, and D. A. Bonn, Phys. Rev. Lett. **93**, 107003 (2004).

[19] D. Dulic, S. J. Hak, D. van der Marel, W. N. Hardy, A. E. Koshelev, Ruixing Liang, D. A. Bonn, and B. A. Willemsen, Phys. Rev. Lett. **86**, 4660 (2001).

[20] H. Shibata, Physica C **367**, 360 (2002).

[21] C. C. Tsuei, J. R. Kirtley, C. C. Chi, L. S. Yu-Jahnes, A. Gupta, T. Shaw, J. Z. Sun, and M. B. Ketchen, Phys. Rev. Lett. **73**, 593 (1994).

[22] J. R. Kirtley, C. C. Tsuei, M. Rupp, J. Z. Sun, L. S. Yu-Jahnes, A. Gupta, M. B. Ketchen, K. A. Moler, and M. Bhushan, Phys. Rev. Lett. **76**, 1336 (1996).

[23] C. C. Tsuei and J. R. Kirtley, Rev. Mod. Phys. **72**, 969 (2000).

[24] A. Sugimoto, T. Yamaguchi, and I. Iguchi, Appl. Phys. Lett. **77**, 3069 (2000).

[25] J. R. Kirtley, C. C. Tsuei and K. A. Moler, Science **285**, 1373 (1999).

[26] A. Sugimoto, T. Yamaguchi, and I. Iguchi, Physica C **367**, 28 (2002).

[27] A. Sugimoto, T. Miyake, T. Takeda, I. Iguchi, and S. Kashiwaya, J. Phys. Soc. Jpn. **41**, L739 (2002).

[28] J. R. Kirtley, K. A. Moler, G. Villard, and A. Maignan, Phys. Rev. Lett. **81**, 2140 (1998).

[29] K. A. Moler, J. R. Kirtley, D. G. Hinks, T. W. Li, and M. Xu, Science **279**, 1193 (1998).

[30] J. R. Clem and M. W. Coffey, Phys. Rev. B **42**, 6209 (1990).

[31] J. R. Kirtley, V. G. Kogan, J. R. Clem, and K. A. Moler, Phys. Rev. B **59**, 4343 (1999).